Colloid Polym Sci (2007) 285:1719–1726
DOI 10.1007/s00396-007-1757-y

SHORT COMMUNICATION

Formation of zinc sulfide and hydroxylapatite nanoparticles in polyelectrolyte-modified microemulsions

Joachim Koetz · Jennifa Baier · Sabine Kosmella

Received: 19 June 2007 / Revised: 27 July 2007 / Accepted: 5 August 2007 / Published online: 12 September 2007

Abstract The paper is focused on the formation of nanoparticles, i.e., zinc sulfide (ZnS) and hydroxylapatite, in a microemulsion template phase consisting of heptanol, water, and a surfactant with a sulfobetaine head group in the absence and presence of an added polyelectrolyte. In the absence of a polyelectrolyte, beside larger particles, spherical ZnS nanoparticles with a diameter below 10 nm can be redispersed after solvent evaporation. In the presence of the synthetic cationic polyelectrolyte poly (diallyldimethylammonium chloride), a reloading of the particle surface is observed, and cationic charged ZnS nanoparticles, of about 5 nm in size, can be redispersed as a main fraction. When hydroxylapatite is formed in the presence of the more stiff biopolymer chitosan hydroxylapatite, hybrid structures were formed. Transmission electron micrographs show fiber-like aggregate structures, consisting of individual small nanoparticles ordered along the polymer chain.

Keywords Nanoparticles · Zinc sulfide · Hydroxylapatite · Microemulsions · Polyelectrolytes

Introduction

The formation of nanoparticles with particle dimensions below 10 nm and nanoparticle superstructures of defined size and morphology is still of growing interest because of the big potential in technological applications [1–4]. For many applications, the synthesis of monodisperse, nanoscalic particles is of key importance because of the special electrical, optical, optoelectronical, and magnetic properties of these nanoparticles, which strongly depend on their dimensions. Uniformly sized semiconductor nanoparticles have attracted special attention because of their use as quantum dots (QDs) [5].

In medical diagnostics and cancer therapy, QDs can be used as optical molecular imaging agents [6–9]. QDs, as novel fluorescence probes, have shown a great potential for biomolecular labeling and cellular imaging. Near-infrared-emitting QDs can be injected into a primary tumor, and the false color image clearly shows transport of the QDs through lymph vessels to a nearly nymph node. Other examples for the use of QDs can be found in the homogeneous rapid detection of nucleic acids using two-color QDs [10] or for the label-free protein detection [11].

In addition, CdS-peptide QDs can be successfully used in analytical chemistry, e.g., for the Cu detection [12] or paraoxon (neurotoxin) detection. Therefore, CdSe QD films [13] or spherical QD bioconjugates [14] can be successfully used. These examples demonstrate only a part of the broad spectrum of applications. QDs are already successfully incorporated in different types of devices, e.g., in semiconductor optical amplifiers for multichannel amplification [15], in slow and fast light devices [16], QD lasers [17], and QD-based immunosensors [18].

One key parameter in the different fields of application is still the stabilization of the nanoparticles. In general, the particles can be electrostatically or sterically stabilized according to the classical rules of colloid stabilization [19]. Therefore, the electrosteric stabilization by means of polyelectrolytes is of special interest because of the combination of both effects [20].

J. Koetz (✉) · J. Baier · S. Kosmella
Institut für Chemie, Universität Potsdam,
Karl-Liebknecht-Str. 24–25, Haus 25,
14476 Potsdam, Germany
e-mail: koetz@rz.uni-potsdam.de

Recently, we have shown that polyelectrolyte-modified microemulsions can be successfully used as a new type of template [21–25]. On the one hand, the polyelectrolytes can control the size and shape of the nanoparticles during the formation process, and on the other hand, the polyelectrolyte can stabilize the individual nanoparticles during the solvent evaporation and redispersion process. We have already shown that this concept can be successfully applied for the preparation of $BaSO_4$ nanoparticles in water-in-oil microemulsions with cationic cetyl trimethylammonium bromide and anionic sodium dodecyl sulfate surfactant molecules [24, 25]. In a sulfobetaine (SB)-based microemulsion the polyelectrolyte can have an additional masking effect opening the possibility to produce spherical magnetite nanoparticles with diameter below 20 nm [26].

The aim of the present study was to use the 3-(*N*,*N*-dimethyldodecylammonio)propanesulfonate-based microemulsion in the presence and absence of cationic polyelectrolytes, i.e., poly(diallyldimethylammonium chloride) (PDADMAC) and chitosan, as a template phase for the formation of ZnS and hydroxylapatite nanoparticles, respectively. The PDADMAC was used as a more flexible synthetic model compound of varying molar mass, and the chitosan as a more stiff biopolymer. In the ZnS nanoparticle formation process, the aim was to produce uniform small nanoparticles. Alternatively, ZnS nanoparticles can be synthesized according to the preparation procedure already described by Baral et al. and Weller et al. [27, 28]. Nowadays, often, ZnS is used as a shell material surrounding more toxic CdSe or CdS nanocrystals [29].

In the hydroxylapatite formation process, especially, the formation of biocompatible nanostructured composites is of special interest, e.g., for an application as dental ceramic material. It has to be mentioned here that, for example, collagene–apatite nanocomposites are of special interest in tissue engineering [30] and nano-hydroxylapatite/polyamide composites as bone-repair material [31].

Experimental

Materials

$PDADMAC_1$, purchased from Aldrich, were purified by ultrafiltration and freeze drying. In addition, we used a sample of higher molar mass ($PDADMAC_2$) as a gift from the Laschewsky group (Fraunhofer Institut für Angewandte Polymerforschung). The average molecular weights (M_w and M_n) of the two PDADMAC samples were determined by gel permeation chromatography (compare Table 1). $Chitosan_1$ and $Chitosan_2$ (Table 1) obtained from the Peter group (Universität Potsdam) were solubilized in 0.025 M HCl or in acetic acid, respectively.

Table 1 Average molecular weights of polyelectrolytes determined by size exclusion chromatography (SEC) or viscometry

Polyelectrolyte	M_n[a] (g/mol)	M_w[a] (g/mol)	M_v[b] (g/mol)	Degree of deacetylation (%)
$PDADMAC_1$	7.000	11.500	–	–
$PDADMAC_2$	31.000	44.900	–	–
$Chitosan_1$	–	–	64.000	93
$Chitosan_2$	–	–	300.000	92

[a] Determined by SEC
[b] Determined by viscometry

The commercially available heptanol (99%+, Fluka), and 3-(*N*,*N*-dimethyldodecylammonio)propanesulfonate (SB, >97%, Fluka) were used without further purification. Water was purified by the water purification system MODULAB™ PureOne (Continental).

Phase diagram

The partial phase diagram was determined optically by titrating the alcohol/surfactant mixture with water. The area of the isotropic L2 phase, constructed from more than 20 measuring points, was determined by adding water drop by drop to the heptanol/SB mixture (Fig. 1). The marked points A, B, and C represent the different composition of the microemulsions used for the nanoparticle formation.

Synthesis of ZnS nanoparticles

Two separately prepared microemulsions (point A, B, or C) containing 20 mmol/L $ZnSO_4$, and 20 mmol/L NaS,

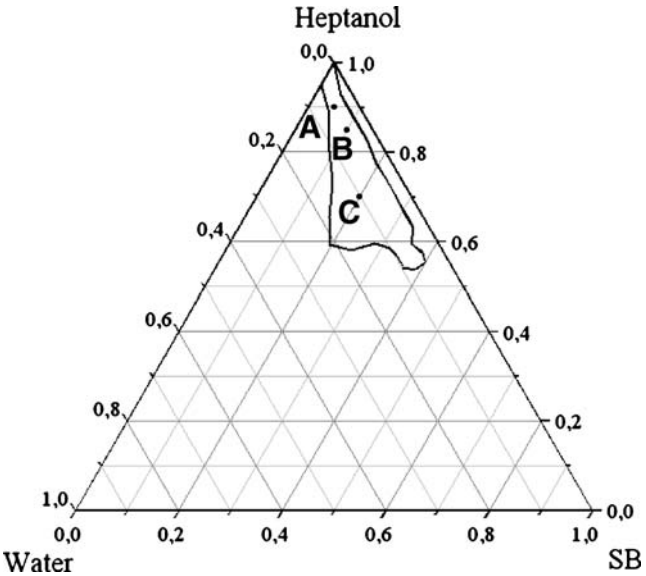

Fig. 1 Partial phase diagram of the ternary water/heptanol/SB system indicating the range of the water-in-oil microemulsion (L2 phase) and the marked compositions A, B, and C

Table 2 DLS characterization of redispersed ZnS nanoparticles after solvent evaporation in absence of a polymer

	Particle size of the main fraction[a] Point A (nm)	$Z_{average}$ Point A (nm)	Particle size of the main fraction[a] Point B (nm)	$Z_{average}$ Point B (nm)	Particle size of the main fraction[a] Point C (nm)	$Z_{average}$ Point C (nm)
without filtration	>300	120–1,200	>400	100–180	>200	68–78
after filtration	4.6±0.9	30–80	5.2±0.8	26–39	7.4±2.7	25–35

[a] Average value from three to five repeat series obtained by automatic peak analysis by intensity

respectively, in the aqueous phase were mixed together. After shaking, the nanoparticles were formed. UV-visible measurements show that after subtraction of the microemulsion reference spectrum, one absorption maximum can be observed at about 230 nm and another one at 260–280 nm. According to the literature values given in the references [32, 33], the peak at 270 nm can be related to ZnS nanoparticles of about 5 nm.

Afterward, the mixture was dried in a vacuum oven at a temperature of 40 °C for 48 h to remove the solvents completely. The remaining powder was redissolved in water by an ultrasound treatment (ultrasound bath or ultrasound finger) and characterized without and after filtration (by using an 800-nm filter) by means of dynamic and electrophoretic light scattering and transmission electron microscopy (TEM).

Synthesis of hydroxylapatite nanoparticles

Route A Three separately prepared microemulsions at a given composition (point A, B, or C) containing the aqueous polymer solution, the 0.1 mol/L $CaCl_2$, and the 0.06 mol/L Na_3PO_4 solution, respectively, in the inner phase were mixed together. After shaking for 2 days, the nanoparticles were formed. Afterward, the mixture was dried in a vacuum oven at a temperature of 40 °C for 48 h to remove the solvents. The remaining powder was redissolved in water with an ultrasound finger and characterized by means of dynamic light scattering and transmission electron microscopy.

Route B Three separately prepared microemulsions at a given composition (point A, B, or C) containing the aqueous polymer solution, 0.1 mol/L $CaCl_2$, 0.06 mol/L NaH_2PO_4, and 1 (or 0.1) mol/L NaOH solution, respectively, in the inner phase were mixed together. After shaking for 2 days, the nanoparticles were formed. Afterward, the mixture was dried in a vacuum oven at a temperature of 40 °C for 48 h to remove the solvents completely. The remaining powder was redissolved in water with an ultrasound finger and characterized by means of dynamic light scattering and transmission electron microscopy.

Characterization of the nanoparticles

Dynamic light-scattering measurements were employed at 25 °C at a fixed angle of 173° (backscattering) by using a Zetasizer 1000 HS (Malvern) equipped with a He–Ne laser (10 mW) and a digital autocorrelator. The average size of the ZnS nanoparticle main fraction (obtained from three to five repeat series) was determined by using an automatic peak analysis by intensity. In addition, the $Z_{average}$ value (independent of the type of data analysis used) was listed.

Electrophoretic light scattering was used to determine the zeta potential of the redispersed nanoparticles. The electrokinetic potential at the effective shear plane between the moveable and nonmoveable part of the double layer was measured by using the Nano Zetasizer (Malvern).

Transmission electron microscopy (EM 902, Zeiss) was used to visualize the morphology and particle size of the nanoparticles formed. Samples were prepared by dropping a small amount of the redispersed aqueous solution on the copper grids, dried, and examined in the electron microscope at an acceleration voltage of 90 kV.

Table 3 DLS characterization of redispersed ZnS nanoparticles after solvent evaporation in the presence of $PDADMAC_1$ (M_n=7.000 g/mol)

	Particle size of the main fraction[a] Point A (nm)	$Z_{average}$ Point A (nm)	Particle size of the main fraction[a] Point B (nm)	$Z_{average}$ Point B (nm)	Particle size of the main fraction[a] Point C (nm)	$Z_{average}$ Point C (nm)
Without filtration	5.1±0.2	65–115	4.7±0.3	6–16	5.0±0.5	45–75
After filtration	4.6±0.3	40–80	5.2±1.0	8–14	4.9±0.4	30–67

[a] Average value from three to five repeat series obtained by automatic peak analysis by intensity

Table 4 DLS characterization of redispersed ZnS nanoparticles after solvent evaporation in presence of $PDADMAC_2$ (M_n=31.000 g/mol)

	Particle size of the main fraction * Point A (nm)	$Z_{average}$ Point A (nm)	Particle size of the main fraction* Point C (nm)	$Z_{average}$ Point C (nm)
without filtration	200±5	100–130	>100	57–64
after filtration	5.0±0.3	31–56	4.8±0.5	9–14

*Average value from 3–5 repeat series obtained by automatic peak analysis by intensity

Results

Microemulsion template phase

Figure 1 shows the optically clear area in the heptanol corner (L2 phase) of the ternary system water/heptanol/SB. When water is substituted by a 1% by weight aqueous PDADMAC solution or a 0.1% chitosan solution, the L2 phase is not changed drastically. Therefore, the nanoparticle formation was realized at the marked points A, B, and C. From Cryo scanning electron microscopy, freeze-fracture TEM, and ultrasound relaxation measurements, we know that the droplet size is between 10 and 40 nm, and from ^{1}H NMR self-diffusion and conductometric measurements, one can conclude that the low-molecular-weight PDADMAC is incorporated into these individual nonpercolated water droplets [21]. The incorporation of the chitosan is much more complicated, and already at a polymer concentration greater than 0.2%, phase separation is observed. One can conclude that the more stiff polymer of significant higher molar mass can only be incorporated into droplet clusters, according to the model already proposed by Meier [34].

ZnS nanoparticle formation

In the microemulsion template phase

The particle size distribution of the redispersed nanoparticles after ultrasound treatment shows two main fraction: one fraction of large particles with particle dimensions above 200 nm and a second particle fraction with particle diameter below 10 nm. Without filtration, the particle fraction with large particle dimensions dominates by the peak analysis by intensity. Turning from point A→B→C, the decrease in the $Z_{average}$ value indicates a trend to smaller particle dimensions. After filtration with an 800-nm filter, the nanoparticle fraction with particle diameter less than 10 nm becomes the main fraction, but the $Z_{average}$ value between 25 and 80 nm demonstrates a still broader particle size distribution. Because the broadness of the $Z_{average}$ value becomes smaller at point B and C, one can conclude that the template effect at these points is better than at point A (Table 2).

By means of electrophoretic light-scattering, a negative zeta potential of −5 mV can be detected for these nanoparticles. Taking into account that the ZnS particles, produced by an adequate particle formation process in water, have a positive zeta potential of +7 mV, one can conclude that the end-standing sulfonate groups of the SB adsorb at the cationic particle surface of the ZnS nanoparticles and form a bilayer with a negative zeta potential of about −5 mV (Table 5).

TEM micrographs show on the one hand larger particles and particle aggregates and on the other hand nanoparticles between 3 and 10 nm, in good agreement with the light-scattering results.

In the PDADMAC-modified microemulsion template phase

When similar experiments were made in the presence of the $PDADMAC_1$, already without filtration, the particle fraction with a mean particle size of 5 nm becomes the dominant one, and the $Z_{average}$ is decreased (Table 3). Especially at point B, the $Z_{average}$ without and after filtration is quite the same, indicating the size-controlling effect of the polycation. This means that in the presence of the polycation, the fraction of larger particles or particle aggregates can be decreased significantly. Based on the positive zeta potential values of 22±5 mV, we can assume that the redispersed nanoparticles are stabilized by a PDADMAC layer. One can conclude that the polycation is adsorbed on the particle surface of the double layer surrounded by ZnS nanoparticles via Coulombic interactions between the PDADMAC and the end-standing sulfobetain headgroups according to the model already discussed in the case of the $BaSO_4$ nanoparticle formation process, described in Scheme 1.

This interpretation is well backed by the TEM micrographs showing spherical nanoparticles with an average

Table 5 Zeta potential of the redispersed ZnS nanoparticles after solvent evaporation in absence and presence of PDADMAC

Aqueous phase	Zeta potential Point A (mV)	Zeta potential Point B (mV)	Zeta potential Point C (mV)
Water	−4.7±0.1	−5.6±0.5	−6.2±1.0
1% $PDADMAC_1$	+18.7±1.3	+23.3±1.3	+26.1±2.8
1% $PDADMAC_2$	+23.8±1.0	–	+27.1±3.8

Scheme 1 Model of the PDADMAC-stabilized nanoparticles

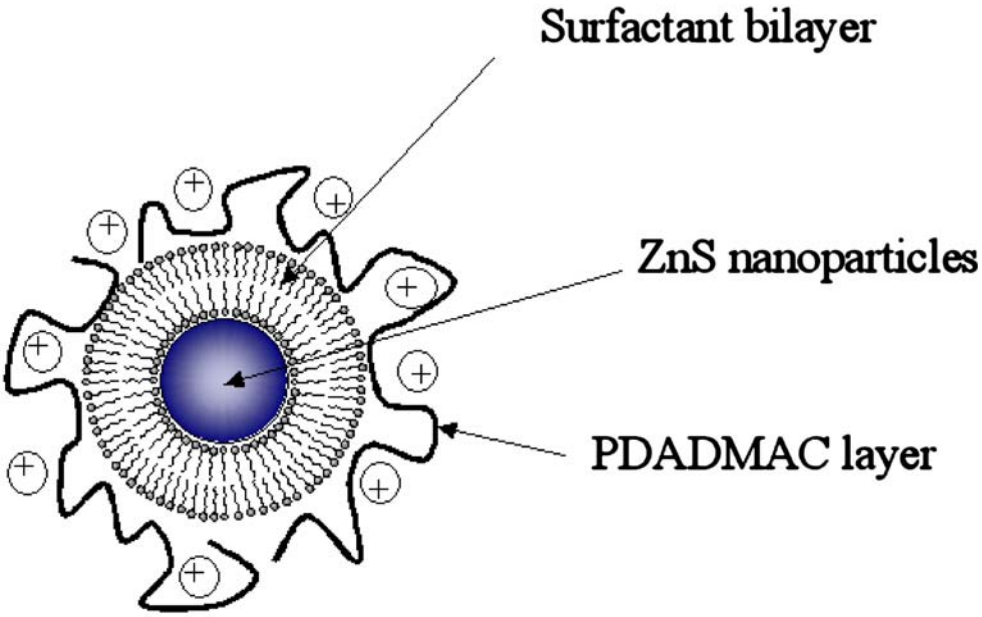

particle size of about 5 nm (Fig. 2) in good agreement with the data obtained by dynamic light scattering.

When the molar mass of the PDADMAC is increased up to M_n=31.000 g/mol (PDADMAC$_2$), the particle formation can be investigated only at point A and C, because of a partial phase separation at point B. The results show a similar trend but not so well pronounced (Table 4). This means that the 5-nm fraction becomes dominant only after filtration, and the $Z_{average}$ between 9 and 14 nm indicates only smaller particle dimensions at point C after filtration (Table 4).

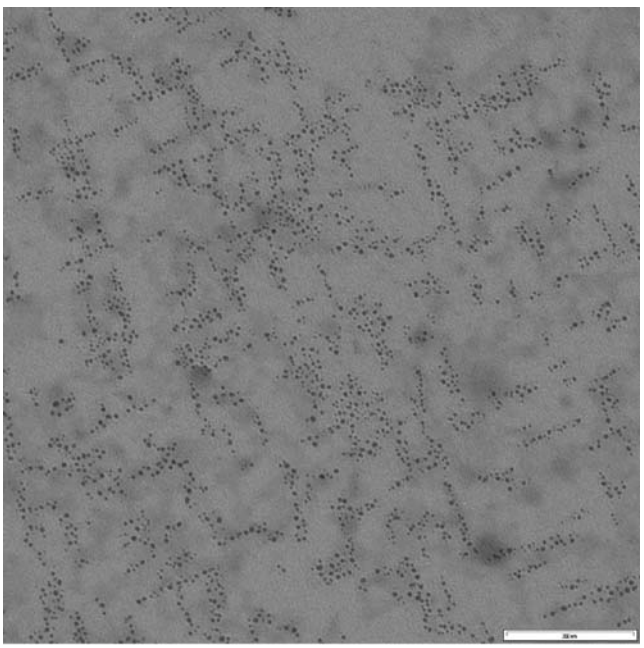

Fig. 2 TEM micrograph of redispersed ZnS nanoparticles synthesized in the PDADMAC-modified microemulsion at point C

In general, the results show that the templating effect of the microemulsion in the absence of the polymer leads to a redispersed particle fraction with particle dimensions below 10 nm, which are stabilized by a surfactant bilayer. Nevertheless, a second fraction with significant larger particle dimensions exists dominating the size distribution determined by dynamic light scattering. When the microemulsion template phase is modified by adding PDADMAC, the small particle fraction becomes more dominant, indicating the size-controlling effect of the polycation. However, the best results were observed at point B by using the low-molecular-weight polycation with M_n=7.000 g/mol (PDADMAC$_1$).

This effect can be explained as follows: the water/surfactant ratio at points B and C equals to 0.5, but the portion of the oil phase at point B is much higher (15% more oil) in comparison to point C. Because of the existence of a water-in-oil microemulsion in both cases, a much better distribution of the water droplets can be assumed at point B. In consequence, the interaction of the water droplets filled with polyelectrolytes and nanoparticles is suppressed. Therefore, the solvent evaporation leads to well-stabilized small nanoparticles.

Inspite of the fact that the templating mechanism is well working for B and C as already discussed, the composition of all three components (water, oil, and surfactant) seems to be of importance and is the most effective one at point B.

The increase in the molar mass of the PDADMAC to M_n= 31.000 g/mol or to M_n=246.000 g/mol (not discussed in more detail) leads to problems in solubilization, resulting in a partial decrease in the L2 phase. Therefore, experiments at point B failed because of a partial phase separation. However, the redispersed nanoparticles produced at points A and C have significant larger dimensions because of a bridging effect of the polycations of higher molar mass.

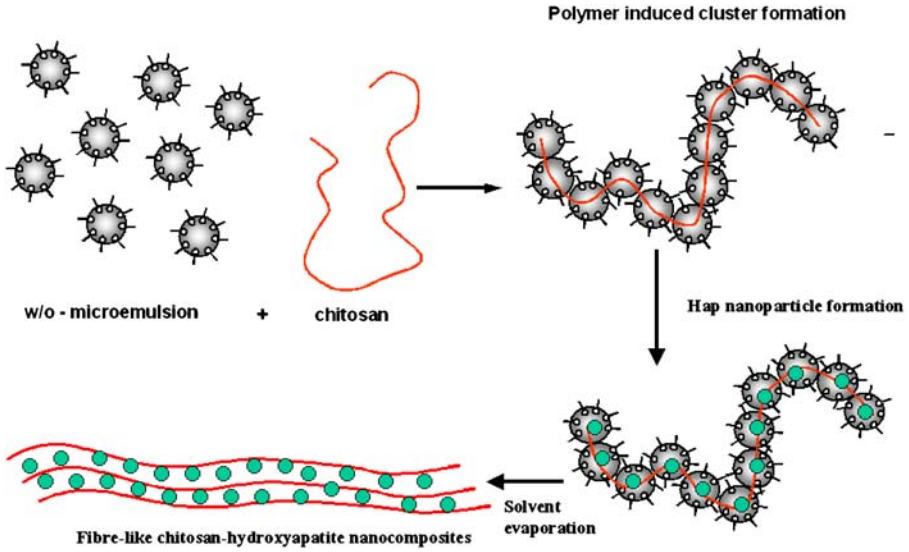

Scheme 2 Model of the formation of chitosan-hydroxylapatite composites

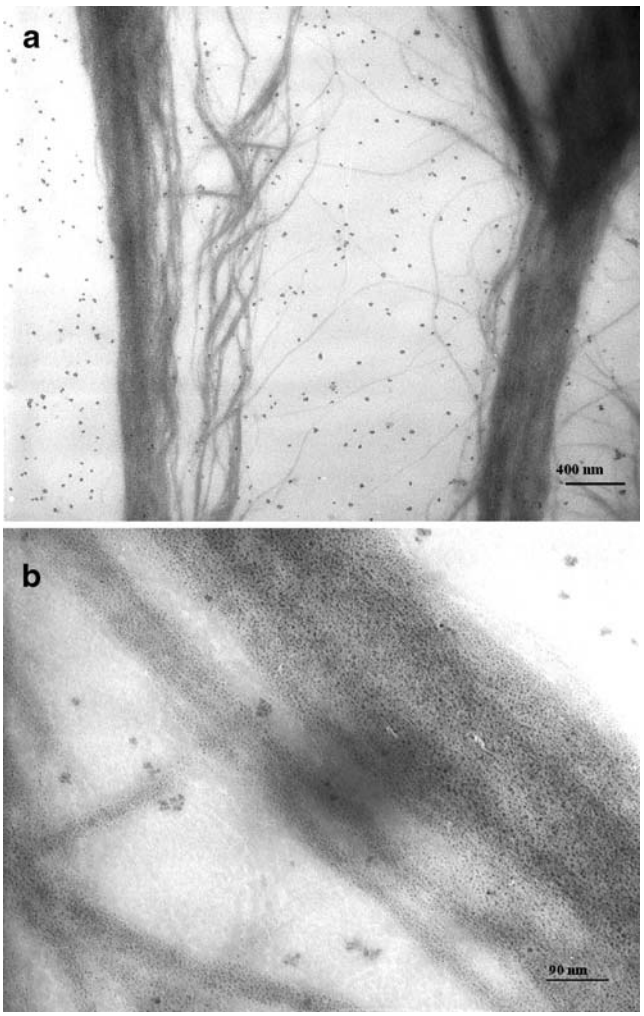

Fig. 3 **a**, **b**. TEM micrographs of redispersed hydroxylapatite nanoparticles synthesized in the chitosan-modified microemulsion at point C

Hap nanoparticle formation

In the microemulsion template phase

First of all, it has to be mentioned here that the formation of hydroxylapatite in microemulsion template phases is much more complicated in comparison to the zinc sulfide formation process. Therefore, we have checked quite different procedures, and finally, two routes were established by mixing three or four microemulsions together. The finally redispersed hydroxylapatite particles are in all cases significantly larger with a mean particle size greater than 300 nm. This means that the templating effect of the microemulsion is quite bad in comparison to the ZnS. One explanation is that a multicomponent mixing procedure is much more complicated and leads to significantly larger aggregates. Another explanation is related to the worse binding conditions for the surfactant molecules on the surface of the hydroxylapatite particles.

In the polymer-modified microemulsion template phase

When adequate investigations were realized in the presence of a polymer, the solubilization capacity strongly depends on the type of polymer used. On the one hand, there is no problem to increase the PDADMAC concentration up to 4%, but on the other hand, the chitosan concentration has to be limited to 0.1–0.2%. This is not surprising because of the more stiff polysaccharide and the higher molar mass. However, additional experiments have shown that also oligomeric chitosan derivatives cannot be incorporated without problems. That means that the solubilization capacity of the DADMAC units is generally much better. In consequence, the chitosan samples used here can be only

solubilized in a microemulsion droplet cluster (compare Scheme 2). The particle dimensions of the finally produced Hap particles in the presence of the chitosan are in the same order as in the unmodified system; this means the particle dimensions detected by dynamic light scattering are in all cases greater than 300 nm, by varying the molar mass of the chitosan or the composition of the microemulsion. After filtration, the count rate is too low for an adequate fit. This means that a smaller nanoparticle fraction, in comparison to the ZnS, does not exist.

TEM micrographs of the redispersed dispersion show on the one hand larger particles of quite different size and shape and on the other hand fibril structures, as to be seen in Fig. 3a. A more detailed look into the "fiber-like" structure (Fig. 3b) indicates that the fibrils consist of individual nanoparticles (<3 nm) ordered along the polymer chain.

Because of the very low polymer concentration, we have to differentiate between the formation of Hap particles in the nonpolymer-filled and polymer-filled microemulsion droplets. In the absence of chitosan, larger Hap particles of different shape (spherical, triangular, or rod-like particles) are formed in similarity to the unmodified microemulsion, having a negative zeta potential.

In the presence of chitosan, things are changed: First of all, the chitosan chain (stiff polysaccharide) induces a cluster formation. When the nanoparticle formation is realized than inside the individual microemulsion droplets, a particle formation along the polymer chain becomes reasonable. After solvent evaporation, a hybrid structure is formed, where the nanoparticles are ordered along the polymer chain, and a fibrillar structure can be observed in the TEM micrographs. The process of hybrid structure formation is demonstrated in Scheme 2.

By substitution of the more stiff chitosan of higher molar mass by the low-molecular-weight $PDADMAC_1$, we observe a quite different behavior. In this case, the polymer can be incorporated into the individual droplets, and polymer-stabilized individual small nanoparticles can be formed. Therefore, we can detect by means of dynamic light-scattering measurements after redispersion nanoparticles with diameter of about 5 nm, which are electrostatically stabilized (positive zeta potential of +26 mV).

Conclusions

The aim of the research was to produce well-stabilized nanoparticles by using polyelectrolyte-modified microemulsions containing heptanol, water, and a surfactant with a SB head group.

First of all, our experiments show that the particle formation process in polyelectrolyte-modified microemulsions strongly depends on the type of polyelectrolyte as well as the type of inorganic material used. When a more flexible polyelectrolyte of low molar mass is used, e.g., the cationic polymer PDADMAC with M_n=7.000 g/mol, ZnS nanoparticles with particle dimensions of 5 nm are predominantly formed, which are well stabilized during the process of solvent evaporation and redispersion. Similar results were observed in the case of hydroxylapatite. This means that the PDADMAC of low molar mass solubilized into individual microemulsion droplets can increase the templating effect of the microemulsion and stabilize the formed nanoparticles during the solvent evaporation and the redispersion process. Therefore, the polymer fulfills indeed the requirements of a size-regulating and stabilizing component in the process of nanoparticle formation and redispersion according to our recently published patent [35]. When the molar mass is increased above a critical value, the polymer can no longer be incorporated into individual droplets, and the size-controlling effect is lost. In addition, the stabilizing effect for individual small nanoparticles during the redispersion is lost because of an enhanced particle aggregation.

When a more stiff polyelectrolyte, i.e., chitosan, of higher molar mass is used, the incorporation of the polymer into individual droplets can no longer be realized, and a cluster formation will be observed. This opens a possibility to produce well-ordered polymer hybrid structures. Therefore, individual Hap nanoparticles can be ordered along the polymer backbone, and fiber-like structures are formed. Such chitosan–Hap superstructures seem to be of special interest in dental applications.

Further experiments will be focused now on the separation of the nanoparticles from the surfactants in the redispersed aqueous solution and the characterization of the optical properties.

Acknowledgment The authors are thankful to B. Tiersch and S. Rüstig (Universität Potsdam) for the TEM micrographs and Andre Laschewsky and Martin Peter (Universität Potsdam) for the supply of the polymer samples.

References

1. Schmid G (2004) Nanoparticles: from theory to application. Wiley, Weinheim
2. Klabunde KJ (2001) Nanoscale materials in chemistry. Wiley, New York
3. Sugimoto T (2001) Monodispersed particles. Elsevier, Amsterdam
4. Kotov NA (2007) Nanoparticle assemblies and superstructures. CRC, Boca Raton
5. Brus LE (1983) J Chem Phys 79(11):5566
6. Park JM, Ikeda DM (2006) Physica Medica 21:7
7. Liu YS, Sun YH, Vernier PT, Liang CH, Chong SYC, Gundersen MA (2007) J Phys Chem C111(7):2872
8. Chatterjee DK, Zhang Y (2007) Sci Technol Adv Materials 8(1–2):131

9. Kumar S, Richards-Kortum R (2006) Nanomedicine 1(1):23
10. Zhang CY, Johnson LW (2006) Analyst 131(4):484
11. Choi JH, Chen KH, Strano MS (2006) J Am Chem Soc 128 (49):15584
12. Gattas-Asfura KM, Leblanc RM (2003) Chem Commun 21:2684
13. Constantine CA, Gattas-Asfura KM, Mello SV, Crespo G, Rastogi VK, Cheng T-C, DeFrank JJ, Leblanc RM (2003) Langmuir 19 (23):9863
14. Ji XJ, Zheng J, Xu J, Rastogi VK, Cheng TC, DeFrank JJ, Leblanc RM (2005) J Phys Chem B 109:3793
15. Wong HC, Ren GB, Rorison JM (2006) IEEE Photonics Technol Lett 18(17–20):2075
16. Chang-Hasnain CJ, Chuang SL (2006) J Lightwave Technol 24 (12):4642
17. Lelarge F, Dagens B, Renaudier J, Brenot R, Accard A, van Dijk F, Make D, Le Gouezigou O, Provost JG, Poingt F, Landreau J, Drisse O, Derouin E, Rousseau B, Pommereau F Duan GH (2007) IEEE J Sel Top Quantum Electron 13(1):111
18. Kerman K, Endo T, Tsukamoto Y, Chikae M, Takamura Y Tamiya E (2007) Talanta 71(4):1494
19. Tadros ThF (1987) Solid/liquid dispersions. Academic, London
20. Koetz J, Kosmella S (2007) Polyelectrolytes and nanoparticles. Springer, Berlin
21. Koetz J, Bahnemann J, Lucas G, Tiersch B, Kosmella S (2004) Colloids Surf A Phys Eng Aspects 250:423
22. Koetz J, Saric M, Kosmella S, Tiersch B (2004) Progr Colloid Polymer Sci 129:95
23. Koetz J, Andres S, Kosmella S, Tiersch B (2006) Compos Interfaces 13(4–6):461
24. Note C, Ruffin J, Tiersch B, Koetz J (2007) J Dispers Sci Technol 28(1):155
25. Note C, Kosmella S, Koetz J (2006) Colloids Surf A Phys Eng Aspects 290:150
26. Baier J, Koetz J, Kosmella S, Tiersch B, Rehage H (2007) J Phys Chem B (in press)
27. Baral S, Fojtik A, Weller H, Henglein A (1986) J Am Chem Soc 108(3):375
28. Weller H, Koch U, Gutierrez M, Henglein A (1984) Ber Bunsenges Phys Chem Chem Phys 88(7):649
29. Talapin DV, Rogach AL, Kornowsky A (2001) Nano Letters 1 (4):207
30. Kim HW, Gu HJ, Lee HH (2007) Tissue Eng 13(5):965
31. Wang XJ, Li YB, Wei J, de Groot K (2002) Biomaterials 23 (24):4787
32. Liveri VT, Rossi M, Arrigo GD, Manno D, Micocci G (1999) Appl Phys A 69:369
33. Nakaoka Y, Nosaka Y (1997) Langmuir 13:708
34. Meier W (1996) Langmuir 12:1188
35. Koetz J, Bahnemann J, Kosmella S, Peter M (2004) PCT: WO 2004/056928 A3